Behind the Skeleton: Unraveling the Genetic Basis of Skeletal Variation in the Coral *Platygyra daedalea*

Shoug Alguthmi
Biological and Environmental Science and Engineering Division, King Abdullah University of Science and Technology, Thuwal, Kingdom of Saudi Arabia https://orcid.org/0009-0006-7219-1995

Sebastian Schmidt-Roach
Ocean Revive, King Abdullah University of Science and Technology, Thuwal, Kingdom of Saudi Arabia

Marcelle Muniz-Barreto
Department of Environmental Protection and Regeneration, Red Sea Global, Umluj, Saudi Arabia

Viswasanthi Chandra
Physical Sciences and Engineering Division, King Abdullah University of Science and Technology, Thuwal, Kingdom of Saudi Arabia

Ronell Sicat
Visualization Core Lab, King Abdullah University of Science and Technology, Thuwal, Kingdom of Saudi Arabia

Thomas Theussl
Visualization Core Lab, King Abdullah University of Science and Technology, Thuwal, Kingdom of Saudi Arabia

Craig T. Michell
craig.michell@kaust.edu.sa

Biological and Environmental Science and Engineering Division, King Abdullah University of Science and Technology, Thuwal, Kingdom of Saudi Arabia https://orcid.org/0000-0003-4706-7256

Manuel Aranda
Biological and Environmental Science and Engineering Division, King Abdullah University of Science and Technology, Thuwal, Kingdom of Saudi Arabia

---

Research Article

Keywords: Corals, Morphological variation, Platygyra daedalea, Red Sea, Population genetics, Genome-wide association study

Posted Date: March 12th, 2026

DOI: https://doi.org/10.21203/rs.3.rs-9092160/v1

Additional Declarations: The authors declare no competing interests.

Abstract

Environmental factors have long been recognized as the primary drivers of intraspecific morphological variation in corals, as demonstrated in numerous species. However, coral calcification is a process that depends on both environmental and biological factors. Understanding the extent to which genetics contributes to morphological variation in corals remains lacking, particularly in corals like *Platygyra daedalea*, a species with complex morphological variation that has been found to be neither induced environmentally nor driven by genetic divergence. To address this gap, we conducted a genome-wide association study using single-nucleotide polymorphism and phenotype data of eight skeletal traits, obtained through restriction enzyme site-associated DNA sequencing and micro-computed tomography, respectively. Here, we demonstrate that genetics contributes to the variation of specific *Platygyra daedalea* skeletal traits, particularly porosity ratio, interseptal distance, and septal thickness. Associated variants were located near genes involved in cell cycle regulation, ciliary function, cytoskeletal rearrangement, and skeletal protein formation. We also found some of these traits to correlate significantly with larger-scale morphological features such as valley width and valley depth, suggesting a potential influence of genetically shaped traits on broader skeletal structure.

INTRODUCTION

Coral reefs are among the most biodiverse ecosystems, supporting at least 25% of marine life while providing us with coastal protection[1,2]. These coral reef frameworks are mainly, albeit not exclusively, built by stony corals, which are increasingly threatened by climate change and ocean acidification[1,3–7]. Understanding how corals build and maintain their skeletons, and how these processes respond to environmental change, is critical for predicting the future of reef ecosystems.

Scleractinian corals generally form their skeletons through the biomineralization of calcium carbonate, facilitated by the calicoblastic epithelium[8–10]. This tissue transfers inorganic and organic components into the extracellular calcifying medium (ECM). The organic matrix (OM) and minerals within the ECM interact to build the skeleton[8–10] along two main axes: lateral thickening and linear extension[4]. Yet, coral skeletal structures vary widely across species, from their microstructure and colony structure to overall growth forms[11].

Skeletal growth rates and characteristics can be influenced by environmental factors such as depth[12], light spectra[13], current intensity[14], and seawater pH[4,5,15,16]. For instance, ocean acidification, driven by elevated atmospheric CO_2 levels, lowers seawater pH and reduces carbonate ion availability[17], decreasing the saturation state of calcium carbonate[8,17]. In response, corals may exhibit reduced calcification rates[15], increased skeletal porosity[4,16], and changes at the molecular level, such as altered DNA methylation patterns[16]. Lateral skeletal thickening in *Porites*, for example, has been found to be sensitive to carbonate ion concentrations[4]. Moreover, *Stylophora pistillata* has shown increases in

skeletal porosity under acidified conditions while maintaining linear extension, possibly through enlarged corallite calyces[15,16] induced by altered cell cycle regulation[16].

Platygyra daedalea is a common reef-building coral throughout the Indo-Pacific region, recognized for its characteristic maze-like skeletal structure[11]. This species exhibits remarkable morphological variation[18,19]. Some coral species with immense morphological variability have long complicated the delineation of taxonomic boundaries[20,21]. Previous studies have sought to determine the drivers of such variation: for example, Miller[18] found that environmental factors along gradients at the Davies Reef in the Great Barrier Reef did not influence *P. daedalea* morphology. Mangubhai *et al*[19] did distinguish two morphotypes in Kenyan *P. daedalea* populations and developed a mathematical equation for field assignment. Additionally, a genetic variance analysis (AMOVA) of microsatellite and internal transcribed spacer (ITS) sequences revealed significant genetic differences between the two morphotypes[19]. However, the morphotypes had no phylogenetic divergence detected using ITS sequences[19]. Moreover, distinguishing between the morphotypes was only possible when both morphological and genetic data were considered together[19]. These findings suggest that *P. daedalea* retains species cohesion despite showing morphological variability. The genetic basis of such intraspecific skeletal variation remains largely unexplored.

Here, we investigated the skeletal variation of *Platygyra daedalea* in the Red Sea, a region that harbors 3.8% of the world's coral reefs and presents steep environmental gradients[22]. We used micro-computed tomography (micro-CT), a high-resolution imaging technique, to quantify skeletal features beyond the limits of traditional methods[23–27]. Additionally, we applied ezRAD sequencing, a cost-effective reduced-representation genomic approach targeting restriction enzyme sites[28], which has been successfully used in coral population studies[29–31]. By integrating these datasets, we examined the genetic basis of skeletal traits, assessed trait correlations, and explored how environmental gradients shape intraspecific skeletal diversity.

MATERIALS AND METHODS

Sample Collection

A total of 90 fragments of *Platygyra daedalea* were collected from five Red Sea locations as follows: Duba (N = 21), Al Wajh (N = 16), Yanbu (N = 18), Al Lith (N = 20), and Southern Farasan Banks (N = 15), see Fig. 1. The sampling sites spanned a range of habitats, including reef slope, reef crest, and seagrass environments (Table 1). Tissue samples were preserved for genetic analysis, and skeletal fragments were bleached using a 20% chlorine solution to remove tissue and dried for morphological examination.

Table 1
Coordinates and habitat types (reef or seagrass) of sample collection sites from five locations along the Red Sea.

Location	Site	Habitat	Latitude (°N)	Longitude (°E)
Duba	Reef 2	Crest	27.29778	35.64389
	Reef 3	Crest	27.27417	35.63722
	Reef 4	Crest	27.30166	35.63361
	Seagrass	Lagoon (onshore)	27.14583	35.73528
Al Wajh	Reef 1	Wall, Crest	25.64139	36.47806
	Reef 2	Wall, Crest	25.50194	36.61833
	Reef 3	Crest	25.30028	36.94972
	Seagrass	Lagoon (offshore)	25.36444	36.90972
Yanbu	Reef 1	Crest	23.79694	37.95528
	Reef 2	Crest	23.76806	37.95667
	Reef 3	Crest	23.65167	38.03361
Al Lith	Reef 1	Wall, Crest	19.77083	39.88972
	Reef 2	Wall, Crest	19.74639	39.90583
	Reef 3	Wall	19.76111	39.95806
Southern Farasan Banks	Reef 1	Wall, Crest	18.27389	40.73028
	Reef 2	Lagoon (offshore)	18.25083	40.73028

Sample Preparation for X-Ray CT Scanning

Skeletal morphological phenotyping was conducted utilizing high-resolution X-ray micro-computed tomography (micro-CT). A subset of 82 *P. daedalea* specimens was phenotyped for skeletal traits: Duba (N = 14), Al Wajh (N = 15), Yanbu (N = 18), Al Lith (N = 20), and Southern Farasan Banks (N = 15). Eight of the ninety collected fragments were unavailable for micro-CT scanning. The bare skeletons were fixed in packaging foam and then inserted into plastic measuring cylinders[32,33] (Figure S1A). Micro-CT scanning was performed using a TESCAN CoreTOM™ CT scanner at 150 kV and 60 W. The images were acquired at a voxel size of 60 µm x 60 µm x 60 µm.

Micro-CT Image Analysis

All image analysis was performed with the software *Avizo 3D* (Thermo Fisher Scientific Inc., Berlin; v2021.2). The TIFF image stack for each scanned cylinder was cropped into individual files for each

coral fragment. These cropped fragments were filtered using *Non-local Means* and *Unsharp Masking* (Avizo module names are italicized in this section). A total of 8 skeletal traits were recorded, as described by Miller[18]: valley width (VW), valley depth (VD), columella width (CW), theca thickness (TT), and septal thickness (ST). In addition, we measured interseptal distance (SS) as the distance between two adjacent septa across an interseptal cavity, measured from the center of the structure, septa teeth count, and porosity ratio.

The macroscopic skeletal traits (CW, TT, ST, and SS) were measured from 2D cross-sections (Fig. 2A), while topological traits (VD and VW) were measured using both 3D reconstructions and cross-sections (Fig. 2C). Septa teeth were counted along one side of a wall in 3D reconstruction (Fig. 2B). Each trait was measured in ten technical replicates and averaged per individual. All measurements, except for the septa teeth count, were made using the Avizo ruler tool. To enhance visibility during analysis, the colormap settings of the *Ortho-slice* and *Volume-Rendering* tools were adjusted (Figure S1B).

Porosity ratio was calculated by segmenting each image, using *Auto-Thresholding*, into two regions: skeletal area (high-threshold) and void area (low-threshold). The skeletal segment was further processed using the *Fill Holes* tool to fill internal skeletal voids. To isolate internal voids, the background was removed from the void segment using the *Border Kill* tool. The porosity ratio was then calculated with the *Volume Fraction* tool by dividing the volume of the void segment (set as the input image) by the volume of the filled skeletal segment (set as the input image mask), providing the ratio of void to skeleton (Figure S2). Boring organisms, including Pyrgomatidae and Dendropoma, were found in the skeletal specimens. Segmentation methods excluded the voids created by these organisms and thus do not affect the calculation of the porosity ratio, as illustrated in Figure S3.

Statistical Analysis of Phenotypic Data

The variance of each trait was compared between the five collection locations in *RStudio*[34] (v2023.06.0). The assumptions for ANOVA, including normality and equal variance, were tested using the Shapiro-Wilk test and the Bartlett test, respectively. If the null hypotheses were not rejected ($p > 0.05$), then parametric tests of ANOVA with Tukey's *post hoc* test were applied. If the assumptions were rejected, non-parametric Kruskal-Wallis tests with Dunn's *post hoc* test were used for the comparison. To evaluate trait correlations, we calculated either Pearson's or Spearman's correlation coefficients, depending on the normality of each trait (Shapiro-Wilk test, $p > 0.05$).

DNA Extraction and ezRAD Library Preparation

Genomic DNA was extracted using a salting out method, commonly known as "Wayne's Method"[35]. DNA concentration was measured using the DNA Broad Range Qubit kit, and the DNA quality was assessed using 0.8% agarose gel electrophoresis.

For the preparation of ezRAD DNA libraries, 100ng of DNA was used following the method of Toonen et al.[28]. The DNA was digested with MboI and Sau3AI enzymes for 6 hours at 37˚C. After digestion, DNA

libraries were prepared using the NEB Ultra II DNA library preparation kit for Illumina. Library size selection was then performed using a 2% agarose gel, where a band of DNA was cut from the gel at 300-500bp. The DNA was recovered from the agarose gel using the QIAGEN MinElute Gel extraction kit following the manufacturer's guidelines. The libraries were then assessed using the Bioanalyzer High sensitivity chip and Qubit. Finally, the libraries were pooled in equimolar ratios and sequenced on the Illumina HiSeq 4000 using the 2 X 150bp chemistry.

Genetic Variant Calling

The primary genetic dataset consisted of 78 individuals: Duba (N = 14), Al Wajh (N = 16), Yanbu (N = 15), Al Lith (N = 19), and Southern Farasan Banks (N = 14). Genetic data for twelve fragments were unavailable, likely due to data loss, DNA extraction failure, or unsuccessful library preparation. A reduced genetic dataset was prepared for the association analysis, including only samples with both genetic and phenotypic data. This reduced dataset comprised 69 individuals: Duba (N = 7), Al Wajh (N = 14), Yanbu (N = 15), Al Lith (N = 19), and Southern Farasan Banks (N = 14).

Genetic variants were obtained first by trimming library adapters and removing low-quality reads from raw reads sequencing data using *Fastp*[36] (v0.23.2). The quality of reads was assessed throughout the workflow using *FASTQC*[37] (v0.12.0). Clean reads were then mapped to the *P. daedalea* reference genome[38] v1.0 with *BWA*[39] (v0.7.17). Then, *Samtools*[40] (v1.16.1) *fixmate* was used to pair complementary reads, and with *Samtools markup*, duplicate reads were removed. *Bcftools*[40] (v1.16) *mpileup* was used to call genetic variants into a raw variant file (VCF). Variants were filtered with *VCFtools*[41] (v0.1.16) using the following parameters: a minor allele frequency of 0.1, a minimum quality of 20, a minimum depth of 10, a maximum depth of 335, and a missing data threshold of 80%. To prune linkage loci, *PLINK*[42] (v2.0) was used with the *indep-pairwise* function, setting the window size to 50 kb, the window step size to 10, and an r^2 threshold of 0.1.

Population Genetics

To estimate population structure, first, a principal component analysis (PCA) was performed using *PLINK pca*. The resulting eigenvalues and eigenvectors were used to plot the PCA in *RStudio* with the *tidyverse* package[43].

A maximum likelihood phylogenetic tree was estimated from the genetic variants (in PHYLIP format obtained by vcf2phylip[44] (v2.9)) using IQTREE[45] (v2.2.6) *model finder*[46] to identify the most suitable substitution model with 1000 bootstrap replications. An additional tree was constructed for the reduced genetic dataset. The resulting trees were visualized in *iTOL*[47] (v6).

Admixture analysis was performed using the sparse non-negative matrix factorization (sNMF) model in the R package *LEA*[48]. The *snmf* function was used to compute cross-entropy values for ancestral populations (K_{sNMF}) ranging from 1 to 10, with ten replicates for each value. The cross-entropy values

were visualized, and the K_{sNMF} corresponding to the lowest cross-entropy was selected as the optimal value of K. The admixture coefficients of the runs with the minimum cross-entropy values were visualized as bar charts and admixture pie charts.

F_{ST} population differentiation statistics were calculated using *VCFtools*, which uses the Weir and Cockerham approach[49]. Pairwise F_{ST} was computed between the three genetic clusters identified from the phylogenetic tree and admixture coefficients of the reduced dataset (Figure S4). SNPs with an $F_{ST} \geq 0.3$ were considered significant as being under selection. Additionally, F_{ST} values were averaged for each pairwise test between the clusters to assess population structure and divergence.

Genome-Wide Association Study

The genome-wide association analysis was conducted using the Latent Factor Mixed Model (*LFMM2*)[48] function from the LEA package in *RStudio*, with the number of latent factors (K) set to three based on the estimated population structure. The significance of the results was computed using *lfmm2.test* function for each trait, and the results were visualized in Manhattan plots. To determine the significance of the associations, we applied a Bonferroni-corrected threshold of p = 0.05.

SNP annotation was performed using *SnpEff*[50] (v5.2c) to predict the potential functional effects of associated variants. A custom *SnpEff* database for *P. daedalea* was built using the reference genome, gene annotations files in the format of 'GFF', and protein sequence[38]. The VCF file was annotated using this custom database.

RESULTS

Morphological Variation Along the Red Sea

To assess the effect of environmental factors on phenotypic variation, we analyzed trait variance for eight skeletal traits across five collection sites along the Red Sea: Duba, Al Wajh, Yanbu, Al Lith, and Southern Farasan Banks (SFB). A one-way ANOVA was applied to traits that met the assumptions of normality and equal variance: theca, thickness (TT), valley width (VW), and septa teeth (Table 2). For traits that violated these assumptions, i.e., porosity ratio, interseptal distance (SS), columella width (CW), and septal thickness (ST), we used Kruskal-Wallis tests (Table 3).

One-way ANOVA showed no significant differences for the traits TT, VW, and septa teeth ($p > 0.05$). Kruskal-Wallis tests showed significant differences for three traits: porosity ratio ($\chi2(4) = 18.8$, $p = 0.00087$); CW ($\chi2(4) = 15.8$, $p = 0.0033$); and ST ($\chi2(4) = 15.9$, $p = 0.0032$). Dunn's post hoc pairwise comparisons indicated significant differences in porosity between Duba and Al Wajh ($p = 0.011$) as well as between Duba and Yanbu ($p = 0.00373$) (Fig. 3A). CW showed significant differences between Duba and Al Lith ($p = 0.00204$) and Duba and Yanbu ($p = 0.0307$) (Fig. 3B). Lastly, ST was significantly different

between SFB and Al Lith ($p = 0.0011$) and SFB and Yanbu ($p = 0.048$) (Fig. 3C). No significant differences were found for SS and VD ($p > 0.05$).

Table 2
One-way ANOVA of variation in morphological traits (TT, VW, septa teeth) among samples from the five locations.

Variable	Condition	N	Average	S	F	P
TT	Duba	14	2.18	0.609	1.145	0.342
	Al Wajh	15	1.95	0.446		
	Yanbu	18	1.82	0.4		
	Al Lith	20	1.85	0.512		
	SFB	15	1.94	0.593		
VW	Duba	14	5.84	0.796	2.275	0.0688
	Al Wajh	15	5.24	0.563		
	Yanbu	18	5.08	0.63		
	Al Lith	20	5.23	0.786		
	SFB	15	5.3	0.899		
Septa teeth	Duba	14	4.51	1.02	0.716	0.584
	Al Wajh	15	4.94	1.01		
	Yanbu	18	4.75	0.797		
	Al Lith	20	4.46	0.917		
	SFB	15	4.57	0.974		

Table 3
Kruskal–Wallis H test results for variation in morphological traits (SS, ST, porosity ratio, VD, CW) among samples from the five locations.

Variable	Condition	N	Mean Rank	Df	χ2	P
SS	Duba	14	47.39	4	1.57	0.814
	Al Wajh	15	40.13			
	Yanbu	18	39.69			
	Al Lith	20	38.15			
	SFB	15	44.00			
ST	Duba	14	38.86	4	15.9	**0.00319**
	Al Wajh	15	43.33			
	Yanbu	18	38.06			
	Al Lith	20	30.05			
	SFB	15	61.53			
Porosity	Duba	14	58.14	4	18.8	**0.000867**
	Al Wajh	15	29.20			
	Yanbu	18	27.94			
	Al Lith	20	48.60			
	SFB	15	45.07			
VD	Duba	14	57.43	4	7.96	0.0932
	Al Wajh	15	39.47			
	Yanbu	18	35.67			
	Al Lith	20	40.20			
	SFB	15	37.40			
CW	Duba	14	60.07	4	15.8	**0.00327**
	Al Wajh	15	44.20			
	Yanbu	18	34.94			
	Al Lith	20	29.25			
	SFB	15	45.67			

Correlation Between Morphological Traits

Pearson correlation was applied to VW, CW, TT, VD, and septa teeth, as the Shapiro-Wilk normality test indicated normal distributions with a p-value > 0.05 and an average of W = 0.98. For ST (W = 0.90), SS (W = 0.90), and porosity ratio (W = 0.67), where normality was rejected ($p < 0.05$), Spearman's correlation was used (Table 4).

Correlation coefficients were computed to assess the linear relationship among the eight traits. Very high positive correlations were found between VD and VW ($r(80) = 0.93$, $p < 0.001$), as well as VD and TT ($r(80) = 0.80$, $p < 0.001$). Additionally, VW was highly positively correlated with TT ($r(80) = 0.71$, $p < 0.001$). Several traits exhibited moderate positive correlations, all statistically significant: porosity with VD ($r(80) = 0.48$, $p < 0.001$), and VW ($r(80) = 0.41$, $p < 0.001$); CW with VW ($r(80) = 0.51$, $p < 0.001$), and VD ($r(80) = 0.58$, $p < 0.001$); VD with SS ($r(80) = 0.43$, $p < 0.001$).

Table 4
Pearson and Spearman* correlation pairwise traits results, with the method chosen based on the Shapiro–Wilk normality test results.

	VW	CW	TT	ST*	SS*	Porosity ratio*	VD	Septa teeth
VW	-	0.51(80)	0.71(80)	0.32(80)	0.31(80)	0.41(80)	0.93(80)	0.02(80)
		p < 0.001	**p < 0.001**	**p = 0.003**	**p = 0.005**	**p < 0.001**	**p < 0.001**	p = 0.87
CW		-	0.28(80)	0.34(80)	0.36(80)	0.18(80)	0.58(80)	0.02(80)
			p = 0.009	**p = 0.002**	**p < 0.001**	p = 0.11	**p < 0.001**	p = 0.85
TT			-	0.34(80)	0.29(80)	0.37(80)	0.80(80)	0.04(80)
				p = 0.002	**p = 0.008**	**p = 0.001**	**p < 0.001**	p = 0.72
ST*				-	0.25(80)	0.11(80)	0.36(80)	-0.13(80)
					p = 0.026	p = 0.33	**p < 0.001**	p = 0.23
SS*					-	0.16(80)	0.43(80)	-0.07(80)
						p = 0.16	**p < 0.001**	p = 0.52
Porosity ratio*						-	0.48(80)	-0.05(80)
							p < 0.001	p = 0.66
VD							-	0.01(80)
								p = 0.89
Septa teeth								-

Population Structure of Red Sea *Platygyra daedalea*

Using an ezRAD sequencing approach, we identified 20,290 high-quality single-nucleotide polymorphisms (SNPs) from 78 individuals. The reduced secondary data set, consisting of 69 individuals, had a total of 20,140 SNPs. Population structure was assessed using admixture and principal component analyses (PCA) with the primary dataset of 20,290 (N = 78). For the admixture analysis, we evaluated clustering for up to ten groups (K = 1–10) using LEA sNMF cross-entropy, which indicated that the optimal K_{sNMF} value is either K = 2 or K = 3. Admixture coefficients at K_{sNMF} = 2, 3, and 4 were visualized alongside a phylogenetic tree (Fig. 4). The samples did not separate based on collection location, and most individuals appeared admixed. However, at K_{sNMF} = 3 and K_{sNMF} = 4, a

stable cluster (yellow) emerged, primarily composed of individuals from Duba and SFB. This cluster was supported by a 94% bootstrap value, suggesting an ancestral relationship among these individuals. When the clustering coefficients were plotted as pie charts for each location sample, Duba and SFB showed a greater proportion of the yellow cluster in comparison to other locations (Fig. 4B).

PCA further revealed that individuals from Duba and SFB exhibited greater genetic variation than individuals from other locations (Fig. 4C and 3D). In PC1 vs. PC2 and PC2 vs. PC3, a subset of individuals from Duba and SFB separated along PC2. Additionally, PC2 versus PC3 showed a separation of a subset of individuals from Al Lith from the larger cluster. These PCA results are consistent with the admixture analysis and phylogenetic tree, supporting $K_{sNMF} = 3$ as the most likely population structure.

To assess whether the genetic clusters belong to a single species, we calculated pairwise F_{ST}, which measures allele frequency differences. The pairwise F_{ST} values were low: $F_{ST} = 0.027$ between populations 1 and 2, $F_{ST} = 0.018$ between populations 1 and 3, and $F_{ST} = 0.017$ between populations 3 and 2. These values indicate minimal genetic differentiation, suggesting that despite some population structure, these groups likely belong to a single species with ongoing gene flow.

Phenotype to Genotype Association

The association between genetic variation and morphological variation in *P. daedalea* was investigated for eight traits, using a Bonferroni-corrected threshold of $p = 2.5 \times 10^{-6}$. Significant associations were identified for three traits: 35 SNPs were associated with SS, 32 SNPs with ST, and 27 SNPs with porosity ratio (Fig. 5). Among the 35 SNPs associated with SS, a total of 45 functional annotations were assigned: 91% had a modifying effect, 55.5% were intergenic, and 15.5% were located upstream of genes. The 32 SNPs associated with ST had 45 annotations, 89% had a modifying effect, 55.5% were intergenic, and 20% were downstream of genes. The 27 SNPs associated with porosity ratio had a total of 38 annotations, of which 89% had a modifying effect, 45% were intergenic, and 18% were upstream of genes. The SNPs associated with phenotypic traits determined by LFMM2 were compared to F_{ST} outliers, and no overlaps were found. Genes located near the associated SNPs had various functions, including roles in processes such as the cell cycle, regulation of cell shape, cilium assembly, and transport. Details of the SNPs associated with porosity ratio, SS, and ST, along with their corresponding gene annotations, are provided in Tables S1, S2, and S3, respectively. However, the exact causal SNPs remain to be identified through further sequencing and analysis, and the precise functions of the associated genes in corals are yet to be determined.

DISCUSSION

Slight Effect of Environmental Gradients on *Platygyra daedalea* Morphology

Here, we analyzed the skeletal variation of *Platygyra daedalea* across the pronounced environmental gradients of the Red Sea, although pinpointing exact causal factors remains challenging due to the lack

of microenvironmental data. Nevertheless, leveraging natural environmental gradients offers a powerful approach, as it mirrors the varied conditions typically explored in laboratory experiments. Several environmental gradients, including alkalinity[51,52], salinity, and annual maximum temperature, occur along the Red Sea, shaped largely by its limited freshwater input and regional climate[22].

The most significant results were observed for porosity, with Duba corals exhibiting significantly higher variation in their porosity ratio compared to nearby locations of Al Wajh and Yanbu. Under lower pH conditions, corals can become more porous[4,5,15,16]. Interestingly, we found that the northernmost corals accounted for most of the study's highly porous corals, contrasting with the Red Sea alkalinity gradient, where northern regions are generally more alkaline than southern regions[51,52]. Corals from other locations followed a more predictable pattern consistent with the alkalinity gradient[51,52], except for a decrease in porosity variation in SFB corals. Columella width displayed a declining trend across the study locations, aside from SFB corals, with a decrease in variation, likely influenced by their proximity to a renewing water source[22]. Septal thickness variation was stable over four locations, with an increase in thickness for SFB corals.

Environmental and depth gradients at Davies Reef in the central Great Barrier Reef had no significant association with *P. daedalea* VW, CW, ST, TT, and VD variation[18]. This further confirms that environmental differences are not the primary driver of most *P. daedalea* morphological variation[18]. However, porosity was not investigated at different depths for this species. The Mediterranean *Balanophyllia europaea* showed a slight decrease in porosity with depth, measured at 1, 11, and 21 meters[12]. However, species-specific sensitivities to environmental conditions and their effects on skeletal morphology were demonstrated in an ex-situ light spectra study[13]. In this experiment, *Acropora formosa* and *Stylophora pistillata* each exhibited distinct morphological changes under three light spectra on a macro and microstructure level[13]. These included variations in theca thickness, septal length, distance among corallites, and their diameter, while porosity remained unchanged[13].

Red Sea *Platygyra daedalea* Populations are Genetically Connected with Slight Structure

Given the skeletal trait differences observed across collection sites, we next examined whether underlying genetic structure could account for the skeletal patterns along the Red Sea. For that, we analyzed the genetic population structure of Red Sea *P. daedalea* using admixture and principal component analyses. Our results indicated widespread genetic admixture among individuals, suggesting a lack of reproductive barriers within this species across the Red Sea. Confirming that the species harbors genetic variation and connectivity throughout the Red Sea. In contrast, *P. daedalea* populations in the Arabian Gulf are highly structured and exhibit limited connectivity[31]. This pronounced structure is likely driven by thermal isolation formed by temperature gradients in the Arabian Gulf, which increase towards the center of the water body[31]. Our findings align with observed genetic connectivity patterns in Red Sea *Pocillopora favosa* (previously *P. verrucosa*[53]), which are influenced by the species reproductive

mode[54]. Like *P. favosa*, *P. daedalea* employs broadcast spawning, releasing eggs and sperm into the water column for external fertilization[54–56].

However, individuals from Duba and SFB exhibit higher genetic diversity, potentially influenced by specific environmental gradients[22,51] or genetic gradients[22] specific to *P. daedalea.* The extreme environmental conditions in Duba and SFB do not seem to reduce the species' genetic diversity through selective pressures. Conversely, the northern region exhibits increased salinity, alkalinity, and lower temperatures[22]. The latter has established the region as a coral refugia, contributing to significantly lower bleaching rates compared to corals in the southern Red Sea[22,57]. These favorable conditions may enhance coral growth and resilience to climate stress[22,57], potentially contributing to Duba maintaining a higher genetic diversity as observed. Moreover, gene flow may have increased the gene pool diversity of SFB, given its proximity to Indian Ocean water inputs. This genetic pattern bears some resemblance to that observed in a genetic clustering of Red Sea *Stylophora pistillata*, which was only present in the southern and northern regions of the Red Sea[54]. However, for *P. daedalea*, the genetic cluster is also present among individuals in the central region, albeit with lower abundance.

Genetic Influence on Coral Morphological Traits

Association analysis of eight quantitative traits revealed strong genetic associations for porosity ratio, septal thickness, and interseptal distance. While previous studies using microsatellite and internal transcribed spacer (ITS) sequences have differentiated two *P. daedalea* morphotypes, these molecular biomarkers required integration with morphological data to effectively distinguish morphotypes[19]. Notably, Mangubhai et al[19] excluded 88 out of 133 *P. daedalea* samples due to intermediate morphologies. In contrast, our study identified traits distributed along a continuum of phenotypes. The quantitative nature of our measurements suggests that, if genetically associated, these traits may be polygenic[58]. We refrained from categorizing corals into morphotypes or genetic groups to enable independent association testing of each trait. By leveraging ezRAD sequencing, which provides high-density single-nucleotide polymorphism (SNP) data[59], we provide a deeper understanding of the relationship between genetic and morphological variation. However, the specific associated genetic variants remain to be identified through higher-resolution sequencing and analyses.

Porosity: The Most Complex of All Skeletal Traits

We identified 27 genetic associations with porosity ratio. The most significantly associated SNP was located 1.41kb downstream of a gene encoding a THAP domain-containing protein 2; the protein localizes in the nucleolus and has DNA and metal ion binding activities[60]. The THAP domain has sequence-specific DNA binding activity[61,62], and it may be involved in various cellular processes, including "proliferation, apoptosis, cell cycle, chromosome segregation, chromatin modification, and transcriptional regulation"[62]. The THAP protein family, which has the THAP domain in common[63],

remains largely understudied, except for THAP1, which plays a fundamental role in cell proliferation and cell-cycle pathways in human endothelial cells[64].

A synonymous variant was identified in a gene encoding a probable DNA polymerase, along with an intronic variant in the gene encoding a translation initiation factor eIF-2B subunit gamma. Additionally, three intergenic variants were found near genes encoding a WW domain-containing oxidoreductase and Tetratricopeptide repeat protein 28, located 7 kb upstream of the latter. WW domain-containing oxidoreductase is essential for normal bone development[65,66] and Tetratricopeptide repeat protein 28 functions during mitosis[67].

Coral skeletons become more porous due to a decrease in skeletal density[24], a response strongly associated with lower pH levels[4,5,15,16,24]. Liew et al.[16] showed that pH induced porosity increase was associated with DNA methylation changes affecting pathways regulating body size and cell cycle[16]. Morphological plasticity has been linked with this induced porosity[15,16], observed to result from initial changes within the coral polyps[16]. We found porosity to have significant moderate positive correlations with valley depth and width, which in turn showed highly significant correlations with other traits.

Although porosity has been shown to arise environmentally[4,5,15,16,24], we also found underlying genetic associations. While the exact functions of the associated proteins remain to be investigated in corals, they are known to have sequence-specific DNA-binding abilities[61,62], functions in the cell cycle[64,67], as a DNA polymerase, and as a translation initiation factor. We hypothesize that the associated SNPs may influence the regulation of the gene expression, potentially causing subtle changes in cell cycle pathways that may affect cell and polyp sizes, ultimately leading to increased porosity.

Linear growth is crucial for corals to compete for light availability required for the coral-*Symbiodiniaceae* symbiosis[68]. Porosity and its associated phenotypes allow maintaining linear extension even with reduced calcification rates under pH stress[4,15,16]. However, *P. daedalea* is not a columnar coral, yet we think, based on the transversal sections (Figure S5), that some void patterns may support linear extension. As *P. daedalea* colonies are mostly massive and hemispherical[11], we hypothesize that wider and deeper valleys may develop as the wall's linear extension increases. However, compared to the high positive correlations between VD, VW, and others, porosity only showed moderate correlations with each VD and VW. This suggests that, in addition to porosity, other factors also play significant roles in VW and VD phenotypic plasticity.

Increased coral porosity can exert both negative[5,69] and positive[5,15,16] impacts on the corals' fitness. Even healthy corals are susceptible to damage and breakage during severe cyclonic events, which are anticipated to increase with climate change[69]. Ocean acidification-driven increases in porosity[4], may lead to more fragile colonies[69]. On the other hand, high porosity acquired by corals can be regarded as a phenotypic adaptation to sea-level rise[16,68,69]. Through this phenotypic plasticity, corals may have the potential to overcome the effects of climate change driven ocean acidification. *Platygyra daedalea* is a

slow-growing coral with a lower porosity ratio than branching corals[15]. If the genetic associations identified in this study are true positives, this may suggest that *Platygyra daedalea* is exhibiting phenotypic plasticity, potentially adopting characteristics of faster-growing coral structures.

The Surprisingly Significant Variation of Septa

We found two septal traits, thickness and distance, to have significant genetic associations. Septa determine the arrangement of mesenteries, which are internal folds of tissue that divide the coelenteron, the body cavity of the coral polyp[70,71]. As Veron et al.[70] describe, “mesenteries give the gastrodermis a large surface area for digestion, photosynthesis, and respiration, and also contain the reproductive organs”. They also form mesenterial filaments that can extend outside the coelenteron for feeding, defense, and wound cleaning[70–72].

Since porosity was unexpectedly linked to cell and polyp phenotypes[16], we hypothesize that variation of septal traits may similarly be driven by mesenterial phenotypes. To our knowledge, no studies have explored these aspects; however, the genetic variants identified in this study suggest a potential link that requires further investigation.

Interseptal distance

Interseptal distance exhibited a strong genetic association with 35 SNPs. Five SNPs were located within genes with distinct functional roles, while two SNPs were positioned near genes with functional annotations in cnidarians. To our knowledge, no prior studies have investigated interseptal distance as a distinct trait in corals. Nevertheless, we hypothesize that certain variants may directly influence variations in biomineralization, while others may impact coral polyp structures.

Skeletal organic matrix protein 5 (SOMP5) is a known component of the coral skeletal proteome, although its specific function remains unclear within the organic matrix[73]. A variant downstream of SOMP5 may contribute to biomineralization variation, influencing the phenotypic variation of *P. daedalea* interseptal distance. Tetratricopeptide repeat protein 21B is part of the intraflagellar transport (IFT) complex, which is essential for the assembly of cilia and flagella[60,74,75]. This protein may affect primary cilia found in the coral ectoderm[76]. Primary cilia are short, non-motile cilia with functions in detecting signals from the surrounding microenvironments[76]. Their presence in the aboral calicoblastic ectoderm suggests that they may serve as sensors of the extracellular calcifying medium environment[76].

Additionally, we speculate that variants within genes encoding E3 ubiquitin-protein ligase (TRIM71) and deoxynucleotide monophosphate kinase (dNMP) may influence variation in reproduction, given their roles in development[77,78] and nucleotide synthesis[79], respectively. Both TRIM71 and dNMP kinase genes exhibited synonymous SNPs associated with interseptal distance. While synonymous mutations are generally considered neutral, they can reduce an organism’s fitness by disrupting binding to regulatory sequences, splicing, and mRNA structure[80–84]. These changes may affect codon bias, gene expression

levels, protein structure, translation efficiency, and RNA stability[80–84]. If synonymous mutations identified in this study have resulted in any phenotypic changes, we presume they would only lead to phenotypic variation rather than gene function changes.

We found intronic variants in the genes coding for Myoferlin[85] and NDRG1[86] to be associated with interseptal distance phenotypes. Myoferlin and NDRG1 are known to play roles in muscle cells and in regulating microtubule dynamics[87], respectively. Specifically, Myoferlin aids in rapid repair and growth by operating in cell division, cell migration, regulation of signaling, and organization of actin dynamics, which promote cytoskeletal rearrangements[85]. As previously mentioned, alterations in cell size and shape have been shown to affect skeletal phenotypes, as does the increase in polyp cell size with larger skeletal calyces[10]. Changes driven by the identified variants may affect cells within the interseptal cavity, potentially altering the distance between adjacent septa. These changes might involve the coral mesenteries, packed between septa, which can elongate their ends to form mesenterial filaments[70,71], driven by cells with muscular activity[88]. Additionally, mesenterial filaments are characterized by ciliation and the presence of stinging cells (nematocysts)[89,90]. We also identified intronic variants in Tetratricopeptide repeat protein 21B and DELTA-alicitoxin-Pse2b, which have been reported to function in cilia assembly and toxin production, respectively[74,91]. While intronic mutations are often considered functionally neutral, they have been found, for example, to influence gene expression and translation efficiency, suggesting that the intronic variants we identified could have similar effects[92,93].

As outlined earlier, based on the functions of the associated genes and the structural roles of septa in relation to mesenteries[70], we believe the variation in septa morphology may be correlated with mesenteries and their filaments. While there is limited knowledge on the cellular and molecular biology of these filaments, we do know they act as defense mechanisms and may confer survival advantages[94,95]. As to retain light availability, larger, slow-growing coral colonies like *P. daedalea* have been observed to use their mesenterial filaments to compete with faster-growing species that try to overshadow them[94,95].

Septal thickness

We found septal thickness (ST) to be genetically associated with 32 SNPs. While ST is a widely examined trait[18,19,96], its connection to mesenteries remains vague, unlike interseptal distance (SS). Our analysis revealed only a weak correlation between ST and SS, suggesting that ST may not be directly influenced by mesenteries. We speculate that as septa become thicker, it may drive mesenteries further apart and provide additional gastrovascular area. However, this will depend largely on additional polyp characteristics such as size and septa number.

Among the identified SNPs, we detected an intronic variant in the gene encoding the BBSome complex member BBS7 protein, with functions in cilium biogenesis [97,98]. In humans, mutations in BBS proteins have been linked to ciliary dysfunction, leading to various features, including skeletal abnormalities[60].

Given that primary cilia may contribute to coral calcification[76], this variant could influence skeletal variation in *P. daedalea*.

Several SNPs were intergenic, including those near genes encoding PAX-interacting protein 1 and Histone lysine acetyltransferase CREBBP, both of which have functions in transcription regulation[60]. Specifically, CREBBP is found to acetylate histones and non-histone proteins[60]. Additionally, RRAGC, which encodes Ras-related GTP-binding protein C, functions as a hydrolase with a crucial role in regulating the mTORC1 signaling cascade[60], which regulates protein synthesis and cell growth[99]. Moreover, Tetratricopeptide repeat protein 28 functions during mitosis[67]. As these proteins play roles in transcriptional regulation, cell growth, and division, we speculate that variations in their genes may potentially affect polyp characteristics and size, much like SNPs associated with porosity ratio. Especially since we found two genes expressing a Tetratricopeptide repeat protein 28 to have genetic associations with both porosity ratio and ST. However, porosity ratio and ST have no correlations based on our results. Thus, the specific relationship between polyp traits and septal thickness remains unclear and will require further investigation, particularly with polyp traits included.

Conclusions

Our study suggests that morphological variation in *Platygyra daedalea* has a genetic basis, indicating that genetics can contribute to species-level morphological variation in corals. While we identified genetic associations for three traits, it is possible that detecting associations for other traits will require a larger sample size or that these traits are more strongly shaped by environmental or epigenetic factors. Notably, the traits with genetic associations were not large structural features, but the latter did correlate with porosity ratio, reinforcing previous findings[15,16]. Annotation of significant SNPs suggests that these variations may impact coral calcification or polyp and mesenterial characteristics, ultimately affecting the skeleton. However, validating these associations will require whole-genome sequencing of individuals to precisely pinpoint potential causal variants through linkage disequilibrium analyses.

The observed morphological variation of *P. daedalea* across nearby reefs, combined with our findings and previous studies[18,19], suggest that environmental factors are not the only influences shaping these phenotypic variations. The lack of significant associations for five traits with environmental gradients indicates that environmental influences vary across traits. Further studies are necessary, particularly through controlled ex situ experiments testing the effects of multiple environmental factors on *P. daedalea.*

Overall, our study underscores the intricate relationship between genetic factors and environmental gradients in shaping coral morphology. The observed phenotype variations suggest that corals develop a range of phenotypes that may enhance their resilience to diverse environmental conditions. These findings provide a clearer understanding of skeletal variation in *P. daedalea* and serve as a starting point for future research on genotype-phenotype-environment associations of coral morphology.

Declarations

Author Contributions

C.M. and M.A. designed the research. S.S.-R. and M.M.-B. collected the samples. C.M. and S.S.-R. performed laboratory work. V.C. scanned corals via Micro-CT. R.S. and T.T. advised on proper image analysis for porosity ratio. S.A. and C.M. did image analysis. S.A. performed bioinformatics analyses and wrote the paper with significant input from C.M. and M.A. All co-authors read and approved the final manuscript.

Acknowledgments

We thank Prof. Francesca Benzoni for her significant revision and suggestions regarding skeletal features. This research was supported by a King Abdullah University of Science and Technology Competitive Research Grant URF/1/4697-01-01 to Aranda, M.

Data Accessibility

Raw sequencing data of ezRAD have been deposited in the NCBI Sequence Read Archive (SRA) under BioProject accession number PRJNA1321291. Micro-CT data, skeletal measurements, and coding script have been deposited in the Dryad repository (Dataset DOI: https://doi.org/10.5061/dryad.9s4mw6mvv).

References

1. Hoegh-Guldberg O, Poloczanska ES, Skirving W, Dove S (2017) Coral Reef Ecosystems under Climate Change and Ocean Acidification. Front Mar Sci 4
2. Reguero BG, Beck MW, Agostini VN, Kramer P, Hancock B (2018) Coral reefs for coastal protection: A new methodological approach and engineering case study in Grenada. J Environ Manage 210:146–161
3. Nelson HR, Kuempel CD, Altieri AH (2016) The resilience of reef invertebrate biodiversity to coral mortality. Ecosphere 7
4. Mollica NR et al (2018) Ocean acidification affects coral growth by reducing skeletal density. *Proceedings of the National Academy of Sciences* 115, 1754–1759
5. Fantazzini P et al (2015) Gains and losses of coral skeletal porosity changes with ocean acidification acclimation. Nat Commun 6:7785
6. Kroeker KJ et al (2013) Impacts of ocean acidification on marine organisms: Quantifying sensitivities and interaction with warming. Glob Chang Biol 19
7. Orr JC et al (2005) Anthropogenic ocean acidification over the twenty-first century and its impact on calcifying organisms. Nature 437

8. Tambutté S et al (2011) Coral biomineralization: From the gene to the environment. J Exp Mar Biol Ecol 408:58–78
9. Allemand D et al (2004) Biomineralisation in reef-building corals: from molecular mechanisms to environmental control. C R Palevol 3:453–467
10. Allemand D, Tambutté É, Zoccola D, Tambutté S (2011) Coral Calcification, Cells to Reefs. in *Coral Reefs: An Ecosystem in Transition* 119–150Springer Netherlands, Dordrecht. 10.1007/978-94-007-0114-4_9
11. Veron JEN, Stafford-Smith M (2000) *Corals of the World*. vol. 1,3Australian Institute of Marine Science, Townsville MC, Qld, Australia
12. Özalp HB, Caroselli E, Raimondi F, Goffredo S (2018) Skeletal growth, morphology and skeletal parameters of a temperate, solitary and zooxanthellate coral along a depth gradient in the Dardanelles (Turkey). Coral Reefs 37:633–646
13. Rocha RJM et al (2014) Contrasting Light Spectra Constrain the Macro and Microstructures of Scleractinian Corals. PLoS ONE 9:e105863
14. Halid N et al (2016) The Effect of Current on Coral Growth Form in Selected Areas of Tioman Island, Pahang. Trans Sci Technol 3:393–400
15. Tambutté E et al (2015) Morphological plasticity of the coral skeleton under CO2-driven seawater acidification. Nat Commun 6:7368
16. Liew YJ et al (2018) Epigenome-associated phenotypic acclimatization to ocean acidification in a reef-building coral. Sci Adv 4
17. Doney SC, Fabry VJ, Feely RA, Kleypas JA (2009) Ocean Acidification: The Other CO 2 Problem. Ann Rev Mar Sci 1:169–192
18. Miller KJ (1994) Morphological Variation in the Coral Genus Platygyra: Environmental Influences and Taxonomic Implications. Mar Ecol Prog Ser 110:19–28
19. Mangubhai S, Souter P, Grahn M (2007) Phenotypic variation in the coral *Platygyra daedalea* in Kenya: morphometry and genetics. Mar Ecol Prog Ser 345:105–115
20. Schmidt-Roach S, Miller KJ, Lundgren P, Andreakis N (2014) With eyes wide open: a revision of species within and closely related to the *Pocillopora damicornis* species complex (Scleractinia; Pocilloporidae) using morphology and genetics. Zool J Linn Soc 170:1–33
21. Schmidt-Roach S et al (2013) Assessing hidden species diversity in the coral *Pocillopora damicornis* from Eastern Australia. Coral Reefs 32:161–172
22. Berumen ML et al (2019) The Red Sea: Environmental Gradients Shape a Natural Laboratory in a Nascent Ocean. in *Coral Reefs of the Red Sea* (eds. Voolstra, C. R. & Berumen, M. L.) vol. 11 1–10
23. Boerckel JD, Mason DE, McDermott AM, Alsberg E (2014) Microcomputed tomography: approaches and applications in bioengineering. Stem Cell Res Ther 5:144
24. Bucher DJ, Harriott VJ, Roberts LG (1998) Skeletal micro-density, porosity and bulk density of acroporid corals. J Exp Mar Biol Ecol 228:117–136

25. Enochs IC, Manzello DP, Wirshing HH, Carlton R, Serafy J (2016) Micro-CT analysis of the Caribbean octocoral Eunicea flexuosa subjected to elevated pCO2. ICES J Mar Sci 73:910–919
26. Roche RC, Abel RA, Johnson KG, Perry CT (2010) Quantification of porosity in *Acropora pulchra* (Brook 1891) using X-ray micro-computed tomography techniques. J Exp Mar Biol Ecol 396:1–9
27. Li Y et al (2021) Micro-CT reconstruction reveals the colony pattern regulations of four dominant reef-building corals. Ecol Evol 11:16266–16279
28. Toonen RJ et al (2013) ezRAD: a simplified method for genomic genotyping in non-model organisms. PeerJ 1:e203
29. Terraneo TI, Arrigoni R, Benzoni F, Forsman ZH, Berumen ML (2018) Using ezRAD to reconstruct the complete mitochondrial genome of *Porites fontanesii* (Cnidaria: Scleractinia). Mitochondrial DNA Part B 3:173–174
30. Terraneo TI et al (2021) Phylogenomics of Porites from the Arabian Peninsula. Mol Phylogenet Evol 161:107173
31. Smith EG et al (2022) Signatures of selection underpinning rapid coral adaptation to the world's warmest reefs. Sci Adv 8
32. Göldner D, Karakostis A, Falcucci A, StyroStone (2022) A protocol for scanning and extracting three-dimensional meshes of stone artefacts using Micro-CT scanners https://www.protocols.io/view/styrostone-a-protocol-for-scanning-and-extracting-b6fsrbne.html StyroStone: A protocol for scanning and extracting three-dimensional meshes of stone artefacts using Micro-CT scanners V.2 PLOS One Peer-reviewed method. https://doi.org/10.17504/protocols.io doi:10.17504/protocols.io
33. Göldner D, Karakostis FA, Falcucci A (2022) Practical and technical aspects for the 3D scanning of lithic artefacts using micro-computed tomography techniques and laser light scanners for subsequent geometric morphometric analysis. Introducing the StyroStone protocol. PLoS ONE 17:e0267163
34. Posit team (2023) RStudio: Integrated Development Environment for R
35. Wilson K et al (2002) Genetic mapping of the black tiger shrimp Penaeus monodon with amplified fragment length polymorphism. Aquaculture 204:297–309
36. Chen S, Zhou Y, Chen Y, Gu J (2018) fastp: an ultra-fast all-in-one FASTQ preprocessor. Bioinformatics 34:i884–i890
37. Andrews S, FastQC (2010) A quality control tool for high throughput sequence data. Babraham Bioinf https://www.bioinformatics.babraham.ac.uk/projects/fastqc/
38. Liew YJ et al (2020) Intergenerational epigenetic inheritance in reef-building corals. Nat Clim Chang 10:254–259
39. Li H, Durbin R (2009) Fast and accurate short read alignment with Burrows–Wheeler transform. Bioinformatics 25:1754–1760
40. Danecek P et al (2021) Twelve years of SAMtools and BCFtools. *Gigascience* 10

41. Danecek P et al (2011) The variant call format and VCFtools. Bioinformatics 27:2156–2158
42. Purcell S et al (2007) PLINK: A Tool Set for Whole-Genome Association and Population-Based Linkage Analyses. Am J Hum Genet 81:559–575
43. Wickham H et al (2019) Welcome to the Tidyverse. J Open Source Softw 4:1686
44. Ortiz E (2023) vcf2phylip v2.9: convert a VCF matrix into several matrix formats for phylogenetic analysis. Preprint at https://github.com/edgardomortiz/vcf2phylip/tree/v2.0
45. Nguyen L-T, Schmidt HA, von Haeseler A, Minh BQ (2015) IQ-TREE: A Fast and Effective Stochastic Algorithm for Estimating Maximum-Likelihood Phylogenies. Mol Biol Evol 32:268–274
46. Kalyaanamoorthy S, Minh BQ, Wong TKF, von Haeseler A, Jermiin LS (2017) ModelFinder: fast model selection for accurate phylogenetic estimates. Nat Methods 14:587–589
47. Letunic I, Bork P (2024) Interactive Tree of Life (iTOL) v6: recent updates to the phylogenetic tree display and annotation tool. Nucleic Acids Res. https://doi.org/10.1093/nar/gkae268
48. Frichot E, François OLEA (2015) An R package for landscape and ecological association studies. Methods Ecol Evol 6:925–929
49. Weir BS, Cockerham CC (1984) Estimating F-Statistics for the Analysis of Population Structure. Evol (N Y) 38:1358
50. Cingolani P et al (2012) A program for annotating and predicting the effects of single nucleotide polymorphisms, SnpEff: SNPs in the genome of Drosophila melanogaster strain w1118; iso-2; iso-3. Fly (Austin) 6:80–92
51. Goyet C, Healy R, Ryan J, Kozyr A (2000) *Global Distribution of Total Inorganic Carbon and Total Alkalinity below the Deepest Winter Mixed Layer Depths*. 10.2172/760546
52. Fine M et al (2019) Coral reefs of the Red Sea — Challenges and potential solutions. Reg Stud Mar Sci 25:100498
53. Oury N, Berumen ML, Paulay G, Benzoni F (2025) One species to rule them all: genomics sheds light on the Pocillopora species diversity and distinctiveness around the Arabian Peninsula. Coral Reefs 44:983–998
54. Buitrago-López C et al (2023) Disparate population and holobiont structure of pocilloporid corals across the Red Sea gradient demonstrate species-specific evolutionary trajectories. Mol Ecol 32:2151–2173
55. Mangubhai S, Harrison PL (2008) Gametogenesis, spawning and fecundity of Platygyra daedalea (Scleractinia) on equatorial reefs in Kenya. Coral Reefs 27:117–122
56. Miller K, Babcock R (1997) Conflicting Morphological and Reproductive Species Boundaries in the Coral Genus *Platygyra*. Biol Bull 192:98–110
57. Osman EO et al (2018) Thermal refugia against coral bleaching throughout the northern Red Sea. Glob Chang Biol 24
58. Das SS (2022) Mendel paved the path toward understanding genetic diseases. Egypt J Med Hum Genet 23:124

59. Baird NA et al (2008) Rapid SNP Discovery and Genetic Mapping Using Sequenced RAD Markers. PLoS ONE 3:e3376
60. Bateman A et al (2023) UniProt: the Universal Protein Knowledgebase in 2023. Nucleic Acids Res 51:D523–D531
61. Bessière D et al (2008) Structure-Function Analysis of the THAP Zinc Finger of THAP1, a Large C2CH DNA-binding Module Linked to Rb/E2F Pathways. J Biol Chem 283:4352–4363
62. Clouaire T et al (2005) The THAP domain of THAP1 is a large C2CH module with zinc-dependent sequence-specific DNA-binding activity. *Proceedings of the National Academy of Sciences* 102, 6907–6912
63. Roussigne M et al (2003) The THAP domain: a novel protein motif with similarity to the DNA-binding domain of P element transposase. Trends Biochem Sci 28:66–69
64. Cayrol C et al (2007) The THAP–zinc finger protein THAP1 regulates endothelial cell proliferation through modulation of pRB/E2F cell-cycle target genes. Blood 109:584–594
65. Aqeilan RI et al (2008) The WWOX Tumor Suppressor Is Essential for Postnatal Survival and Normal Bone Metabolism. J Biol Chem 283:21629–21639
66. Chang N-S et al (2001) Hyaluronidase Induction of a WW Domain-containing Oxidoreductase That Enhances Tumor Necrosis Factor Cytotoxicity. J Biol Chem 276:3361–3370
67. Izumiyama T, Minoshima S, Yoshida T, Shimizu N (2012) A novel big protein TPRBK possessing 25 units of TPR motif is essential for the progress of mitosis and cytokinesis. Gene 511:202–217
68. Law MT, Huang D (2023) Light limitation and coral mortality in urbanised reef communities due to sea-level rise. Clim Change Ecol 5:100073
69. Hoegh-Guldberg O et al (2011) Secretariat of the Pacific Community, Noumea, New Caledonia,. Vulnerability of coral reefs in the tropical Pacific to climate change. in *Vulnerability of Tropical Pacific Fisheries and Aquaculture to Climate Change* (eds. JD Bell, JE Johnson & AJ Hobday) 251–296
70. Veron JEN, Stafford-Smith MG, Turak E, DeVantier LM (2024) Corals of the World. *Accessed 7/2/* Version 0.01Beta. http://coralsoftheworld.org/v0.*01(Beta). (To go to the current version access: http://coralsoftheworld.org)* (2024)
71. Mohan PM, Karuna Kumari R Conservation of Coral Reef Environment: Perspectives for Tropical Islands. in *Biodiversity and Climate Change Adaptation in Tropical Islands* 725–744 (Elsevier, 2008). 10.1016/B978-0-12-813064-3.00026-0
72. Lewis BM, Suggett DS, Prentis PJ, Nothdurft LD (2022) Cellular adaptations leading to coral fragment attachment on artificial substrates in Acropora millepora (Am-CAM). Sci Rep 12:18431
73. Ramos-Silva P et al (2013) The Skeletal Proteome of the Coral Acropora millepora: The Evolution of Calcification by Co-Option and Domain Shuffling. Mol Biol Evol 30:2099–2112
74. Hirano T, Katoh Y, Nakayama K (2017) Intraflagellar transport-A complex mediates ciliary entry and retrograde trafficking of ciliary G protein–coupled receptors. Mol Biol Cell 28:429–439

75. Ishikawa H, Marshall WF (2017) Intraflagellar Transport and Ciliary Dynamics. Cold Spring Harb Perspect Biol 9:a021998
76. Tambutté E, Ganot P, Venn AA, Tambutté (2021) A role for primary cilia in coral calcification? Cell Tissue Res 383:1093–1102
77. Lin Y-C et al (2007) Human TRIM71 and Its Nematode Homologue Are Targets of let-7 MicroRNA and Its Zebrafish Orthologue Is Essential for Development. Mol Biol Evol 24:2525–2534
78. Roush S, Slack FJ (2008) The let-7 family of microRNAs. Trends Cell Biol 18:505–516
79. Van Rompay AR, Johansson M, Karlsson A (2000) Phosphorylation of nucleosides and nucleoside analogs by mammalian nucleoside monophosphate kinases. Pharmacol Ther 87:189–198
80. Wang S, Li L, Tao R, Gao Y (2017) Ion channelopathies associated genetic variants as the culprit for sudden unexplained death. Forensic Sci Int 275:128–137
81. Cannarozzi G et al (2010) A Role for Codon Order in Translation Dynamics. Cell 141:355–367
82. Tuller T et al (2010) An Evolutionarily Conserved Mechanism for Controlling the Efficiency of Protein Translation. Cell 141:344–354
83. Maraia RJ, Iben JR (2014) Different types of secondary information in the genetic code. RNA 20:977–984
84. Duan J, Antezana MA (2003) Mammalian Mutation Pressure, Synonymous Codon Choice, and mRNA Degradation. J Mol Evol 57:694–701
85. Zhu W et al (2019) Myoferlin, a multifunctional protein in normal cells, has novel and key roles in various cancers. J Cell Mol Med 23:7180–7189
86. Kim K et al (2004) Function of Drg1/Rit42 in p53-dependent Mitotic Spindle Checkpoint. J Biol Chem 279:38597–38602
87. Becker R, Leone M, Engel F (2020) Microtubule Organization in Striated Muscle Cells. Cells 9:1395
88. Leclère L, Röttinger E (2017) Diversity of Cnidarian Muscles: Function, Anatomy, Development and Regeneration. Front Cell Dev Biol 4
89. Duros RK (1973) Mesenterial filaments from *Manicina areolata* (linn). Fla Sci 36:164–172
90. Environmental causes of dermatitis. in (2006) Tropical Dermatology. Elsevier, pp 439–467. 10.1016/B978-0-443-06790-7.50039-9
91. Nagai H et al (2002) Novel proteinaceous toxins from the nematocyst venom of the Okinawan sea anemone *Phyllodiscus semoni* Kwietniewski. Biochem Biophys Res Commun 294:760–763
92. Rigau M, Juan D, Valencia A, Rico D (2019) Intronic CNVs and gene expression variation in human populations. PLoS Genet 15:e1007902
93. Shaul O (2017) How introns enhance gene expression. Int J Biochem Cell Biol 91:145–155
94. Lang JC (1970) Inter-specific aggression within the scleractinian reef corals. [Doctoral dissertation, Yale University].ProQuest Dissertations & Theses. (Yale University, United States -- Connecticut
95. Connell JH (1973) Population ecology of reef-building corals. in *Biology and Geology of Coral Reefs* 205–245Elsevier. 10.1016/B978-0-12-395526-5.50015-8

96. Dávalos-Dehullu E, Hernández-Arana H, Carricart-Ganivet JP (2008) On the causes of density banding in skeletons of corals of the genus Montastraea. J Exp Mar Biol Ecol 365:142–147
97. Seo S et al (2011) A Novel Protein LZTFL1 Regulates Ciliary Trafficking of the BBSome and Smoothened. PLoS Genet 7:e1002358
98. Nachury MV et al (2007) A Core Complex of BBS Proteins Cooperates with the GTPase Rab8 to Promote Ciliary Membrane Biogenesis. Cell 129:1201–1213
99. Crino PB (2016) The mTOR signalling cascade: paving new roads to cure neurological disease. Nat Rev Neurol 12:379–392

Figures

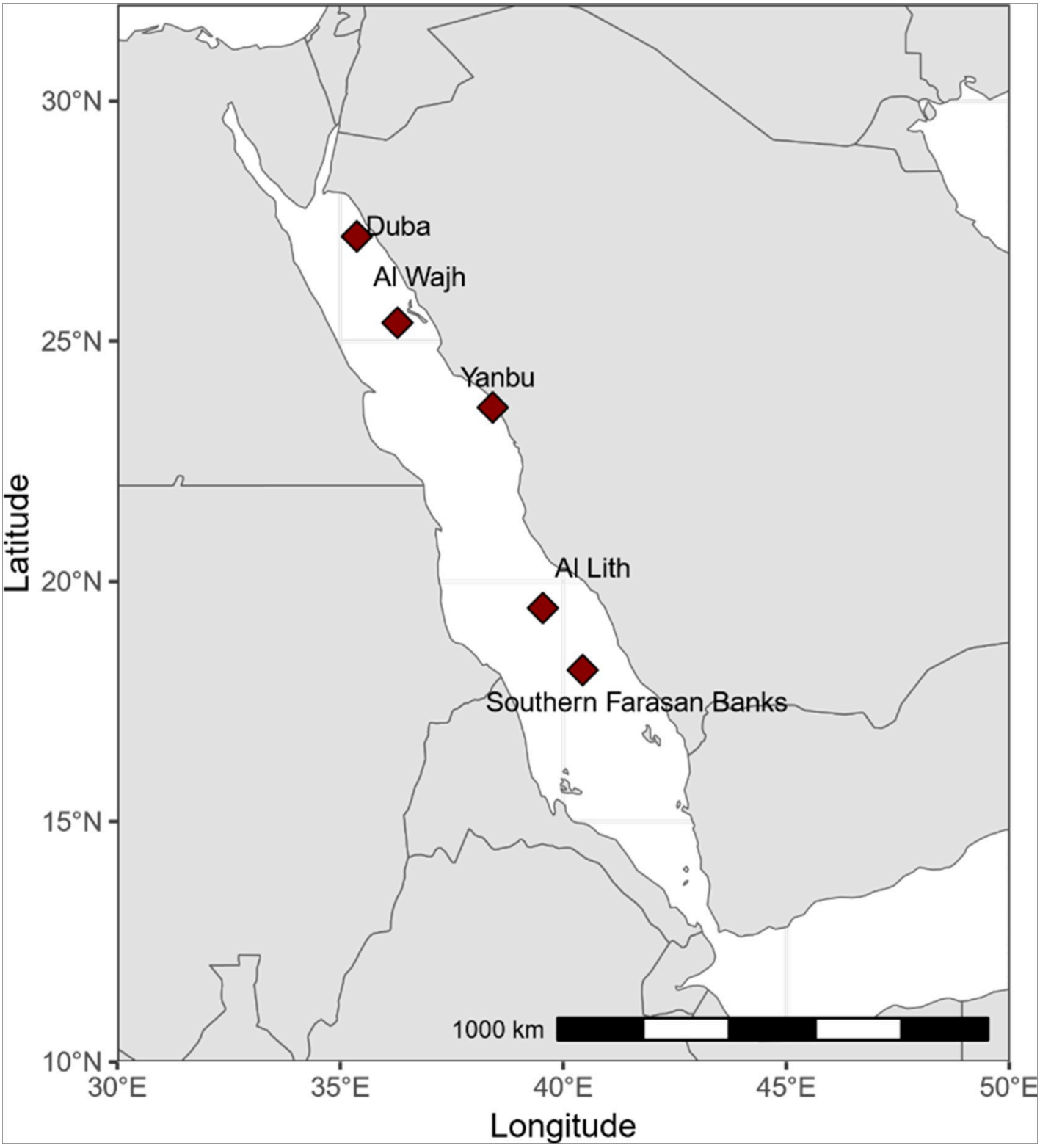

Figure 1

***Platygyra daedalea* sampling locations.** Sampling locations along the Red Sea (North to South): Duba, Al Wajh, Yanbu, Al Lith, and Southern Farasan Banks.

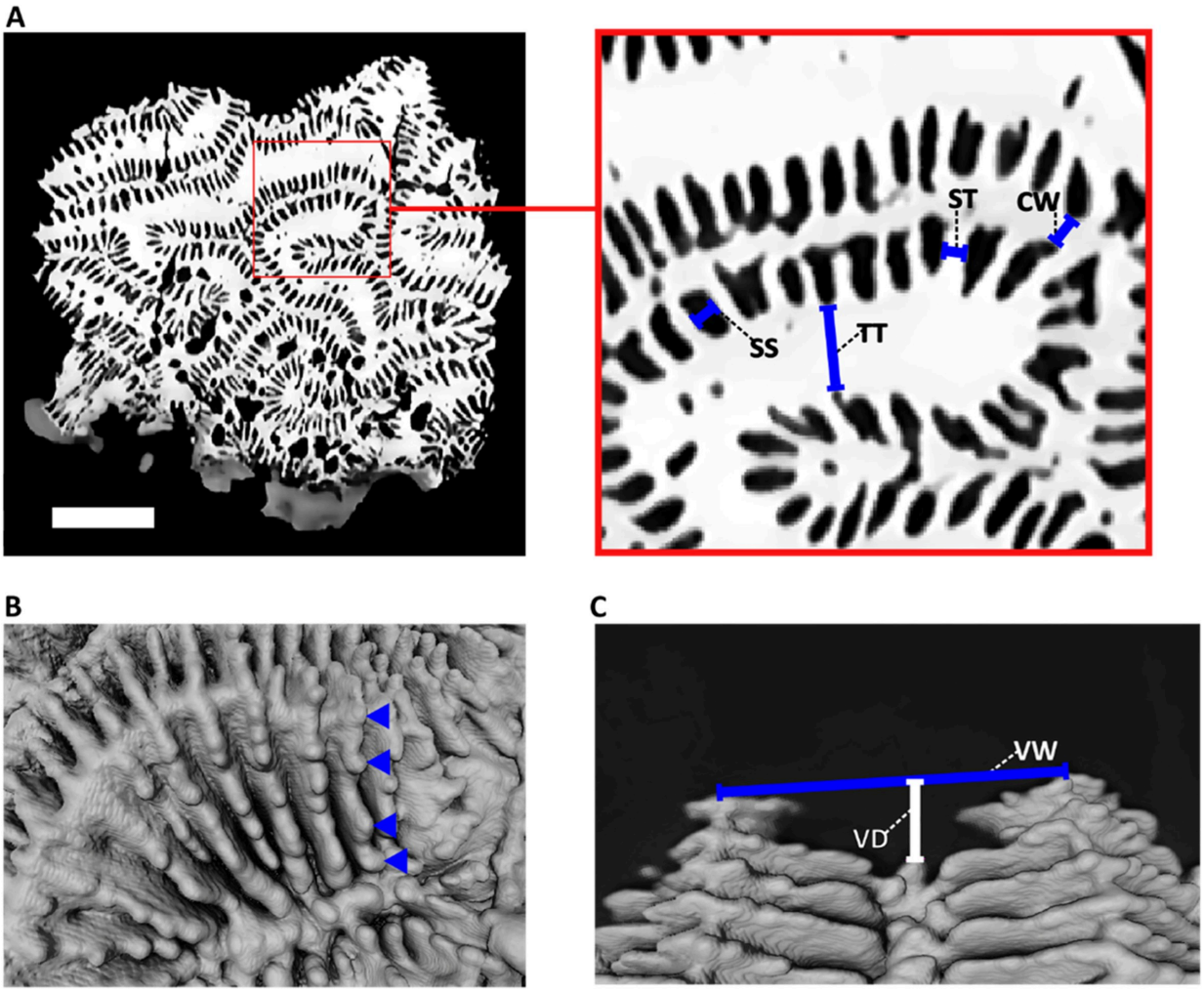

Figure 2

Skeletal trait measurements. A. Cross-section showing trait measurements: columella width (CW), theca thickness (TT), septal thickness (ST), interseptal distance (SS). B. Septa teeth counted along one side of the wall. C. Valley depth and width indicated by vertical and horizontal lines, respectively. Scale bar = 10 mm.

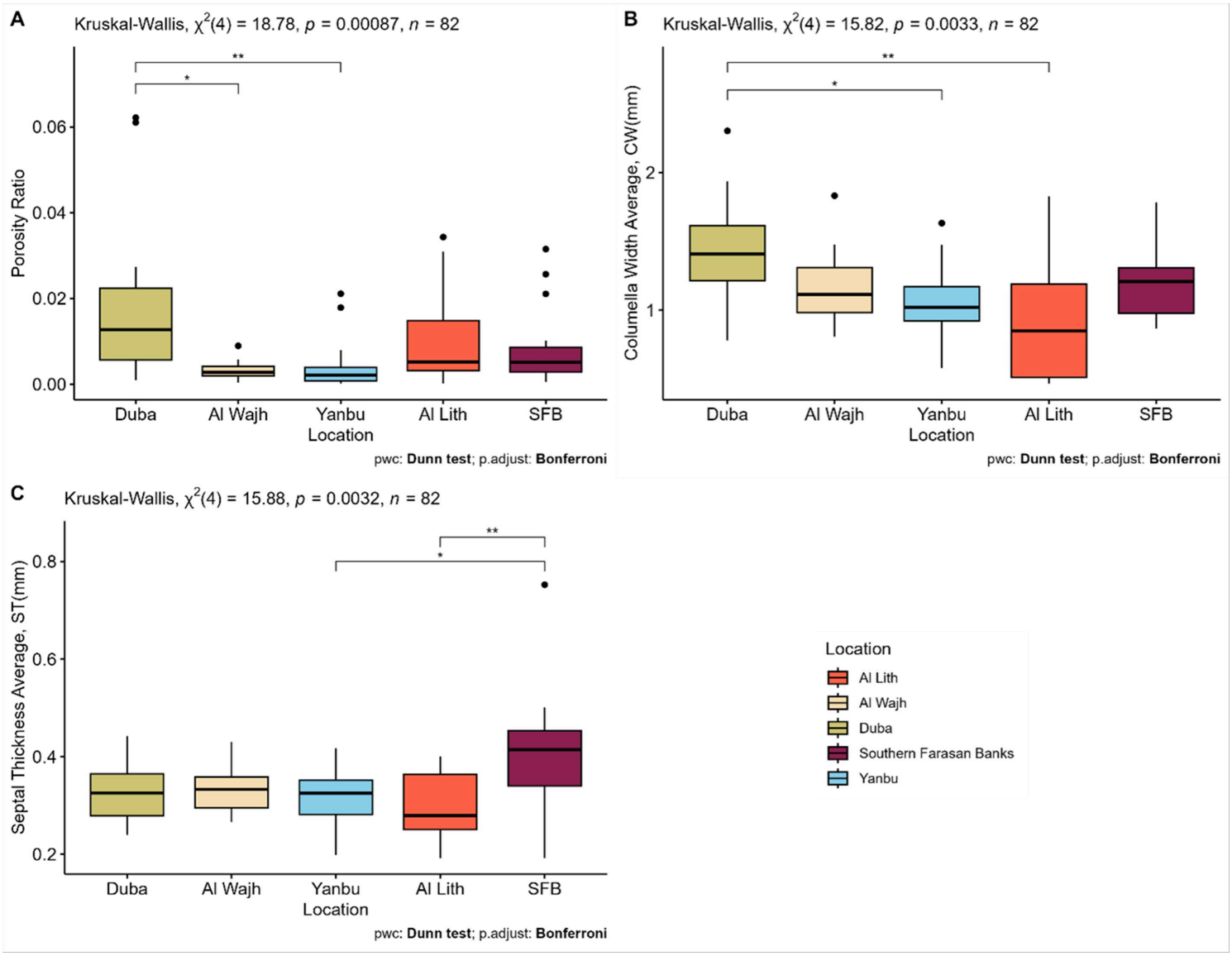

Figure 3

Skeletal traits variation across five Red Sea locations. The locations from north to south of the Red Sea: Duba N = 14 (green), Al Wajh N = 15 (beige), Yanbu N = 18 (blue), Al Lith N = 20 (red), and Southern Farasan Banks N = 15 (purple). Kruskal-Wallis for A. porosity ratio, B. columella width average (mm), and C. septal thickness average (mm).

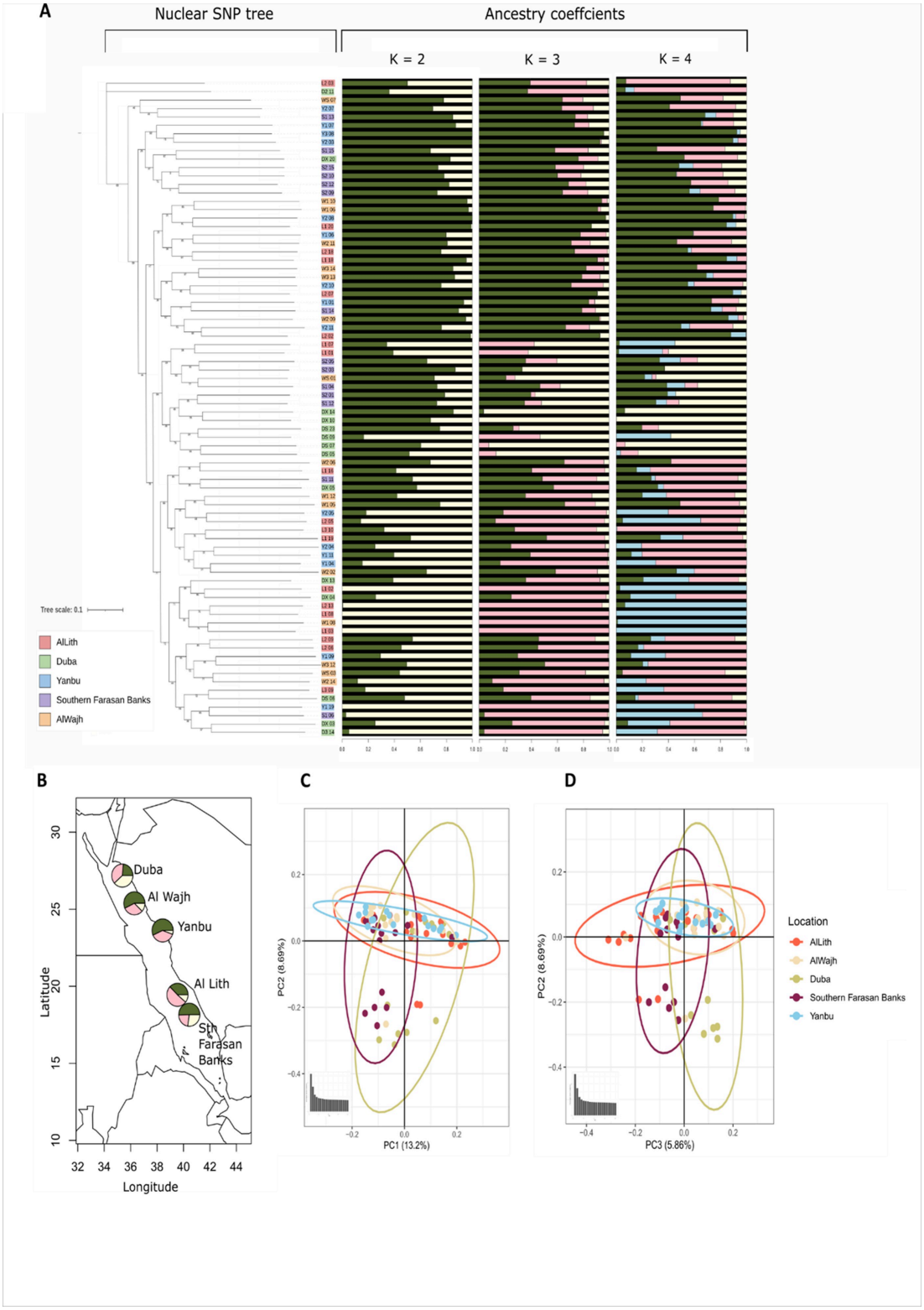

Figure 4

Population structure of Red Sea *Platygyra daedalea*. A. maximum likelihood nuclear tree with admixture proportions for each individual in barcharts at each K = 2,3,4; B. LEA analyses indicating admixture proportions for each population in a pie chart on the Red Sea map, with Duba (N = 14), Al Wajh (N = 16), Yanbu (N = 15), Al Lith (N = 19), and Southern Farasan Banks (N = 14). C., D. Principal components analysis plots of PC1 vs. PC2 and PC2 vs. PC3.

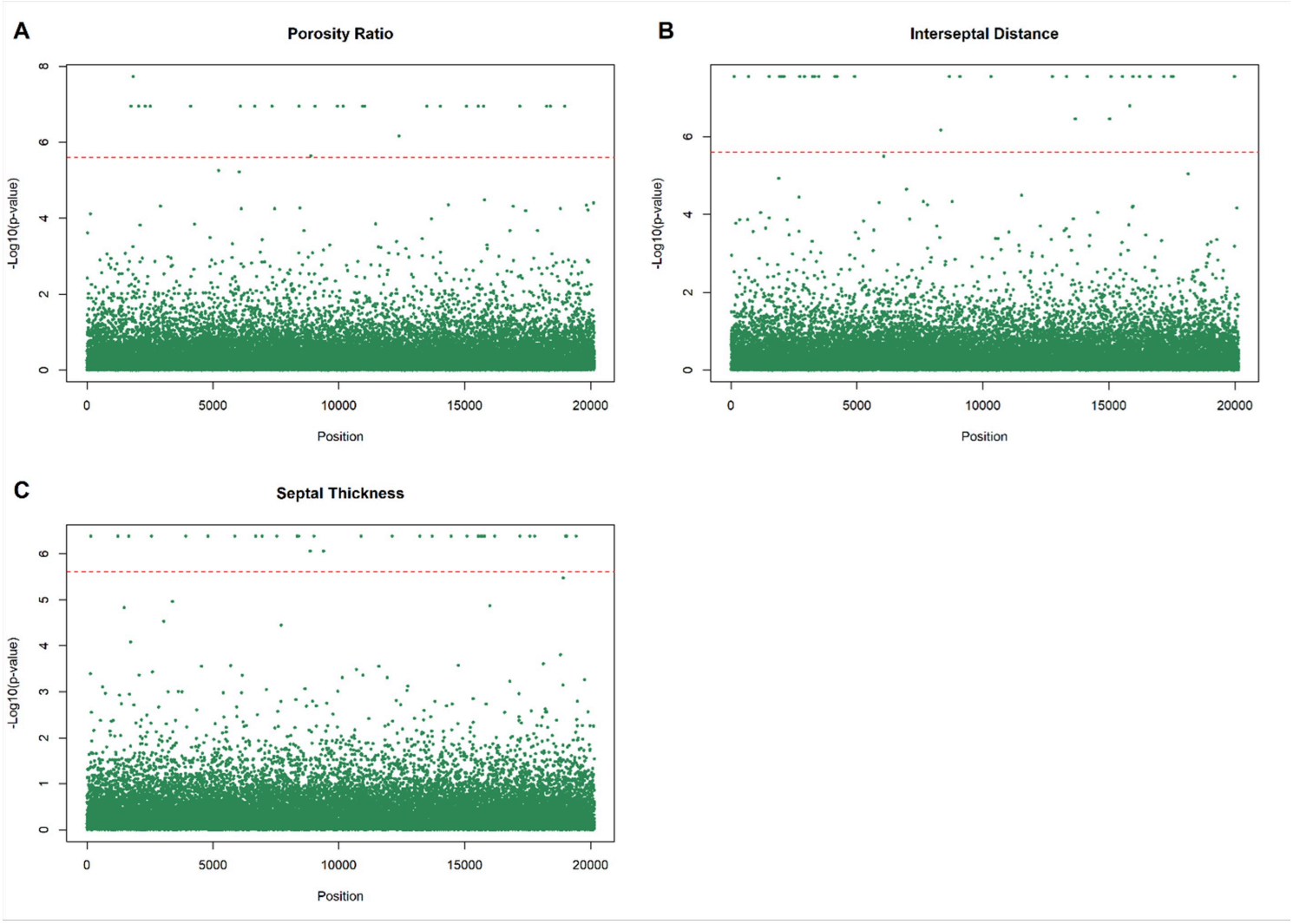

Figure 5

Genome-wide association analysis for *Platygyra daedalea* skeletal traits. A. porosity ratio, B. interseptal distance, and C. septal thickness. The X-axis shows the positions of the genetic variants. The Y-axis shows -Log10 of the p-values. The dotted line indicates the threshold used of Bonferroni-corrected alpha of 0.05.

Supplementary Files

This is a list of supplementary files associated with this preprint. Click to download.

- SupplementalfiguresofBehindtheSkeleton.docx
- TableS1.xlsx
- TableS2.xlsx
- TableS3.xlsx